WAVELETS AND ADAPTED WAVEFORM ANALYSIS

Ronald R. Coifman* and M. Victor Wickerhauser†

*Department of Mathematics
Yale University
New Haven, CT 06520

†Department of Mathematics
Washington University
St. Louis, MO 63130

Abstract. Our goal is to describe tools for adapting methods of analysis to various tasks occuring in harmonic and numerical analysis and signal processing. The main point of this presentation is that by choosing an orthonormal basis, in which space and frequency are suitably localized, one can achieve both understanding of structure and efficiency in computation. We describe a fingerprint image segmentation algorithm, an alternative factorization for the FFT, and a wavelet-based denoising algorithm.

Our goal is to describe tools for adapting methods of analysis to various tasks occurring in harmonic and numerical analysis and signal processing. The main point of this presentation is that by choosing an orthonormal basis, in which space and frequency are suitably localized, one can achieve both understanding of structure and efficiency in computation.

In fact we claim that the search for computational efficiency is intimately related to efficiency in representation (i.e., compression) and to pattern extraction, or structural understanding.

Traditionally in PDE and Harmonic Analysis, microlocalization is the main tool for structural understanding of operators. This is done by choosing appropriate partitions of unity in phase space—decomposition of phase space into cells. The waveform analysis approach provides a numerical recipe for microlocalization, in which the partitions are

*Research supported in part by DARPA and NSF. †Research supported in part by AFOSR.

computed to achieve maximum efficiency in describing interactions. Not only does this approach shed light on classical analysis methods, it also suggests new methods of organization and analysis of operators. These include nonstandard forms and discrete phase space approximations. Our goal is to introduce a variety of techniques permitting the mathematician, scientist or engineer to choose the appropriate analysis method in this catalogue of tools and apply it to practical problems.

In the adapted waveform transform (AWT) method the user is provided with a collection of standard libraries of waveforms—wavelets, wavelet-packets, windowed trigonometric waveforms—which can be chosen to fit specific classes of signals. These libraries come equipped with fast numerical algorithms, enabling real-time implementation of a variety of analysis and signal processing tasks such as data compression, parameter extraction for recognition and diagnostics, and fast transformation and manipulation of digital data.

The process of analysis is usually done by comparing acquired segments of data with stored waveforms. The numerical comparison algorithm itself is fast and perfectly conditioned, always being a factored sparse orthogonal transformation. The most efficient orthonormal basis for compression of the signal is selected and used to extract and manipulate relevant features.

A calculus in compressed variables has been developed enabling the implementation of adapted transform methods for fast numerical algorithms useful for data manipulation and for large scale computation.

Windowed FFT and Adapted Window Selection. To illustrate our procedures we start with a description of an algorithm to compute the Fourier expansion of a function on $[0, 2]$ from the Fourier expansion of its restrictions to $[0, 1]$ and $[1, 2]$.

Let f be defined on $[0, 2]$ and write $f = f^0 + f^1$, where

$$f^0 = \begin{cases} f & x \in [0, 1] \\ 0 & x \notin [0, 1]. \end{cases}$$

We want to compute

$$\hat{f}_m = \frac{1}{\sqrt{2}} \int_0^2 f(t) e^{-2\pi i m \frac{t}{2}}\, dt$$

in terms of

$$\hat{f}_n^0 = \int_0^1 f(t) e^{-2\pi i n t}\, dt \qquad \text{and} \qquad \hat{f}_n^1 = \int_1^2 f(t) e^{-2\pi i n t}\, dt.$$

Clearly, when $m = 2n$ we have

$$\boxed{\hat{f}_{2n} = \frac{1}{\sqrt{2}} \{\hat{f}_n^0 + \hat{f}_n^1\}}.$$

For $m = 2n + 1$ we define

$$d_n = \frac{1}{\sqrt{2}} \{\hat{f}_n^0 - \hat{f}_{n+1}^1\}$$

and find

$$\boxed{\hat{f}_{2n+1} = \frac{1}{\pi i} \sum \frac{d_k}{(n - k + \frac{1}{2})}}.$$

In fact,

$$\hat{f}_{2n+1} = \frac{1}{\sqrt{2}} \int_0^1 [f(t) - f(t+1)] e^{-i\pi t} e^{-2\pi i n t}\, dt.$$

Since d_n are the Fourier coefficients on $[0, 1]$ of $f(t) - f(t+1)$, and $\frac{1}{\pi i (n + \frac{1}{2})}$ are the coefficients of $e^{-i\pi t}$, we obtain the coefficients of $\hat{f}_{2n+1}$ by convolving these sequences. Yet another way to compute $\hat{f}_{2n+1}$ is to compute the inverse transform on $[0, 1]$ of d_n, multiply by $e^{-it/2}$ and recompute the transform on $[0, 1]$.

Figure 1. Schematic description

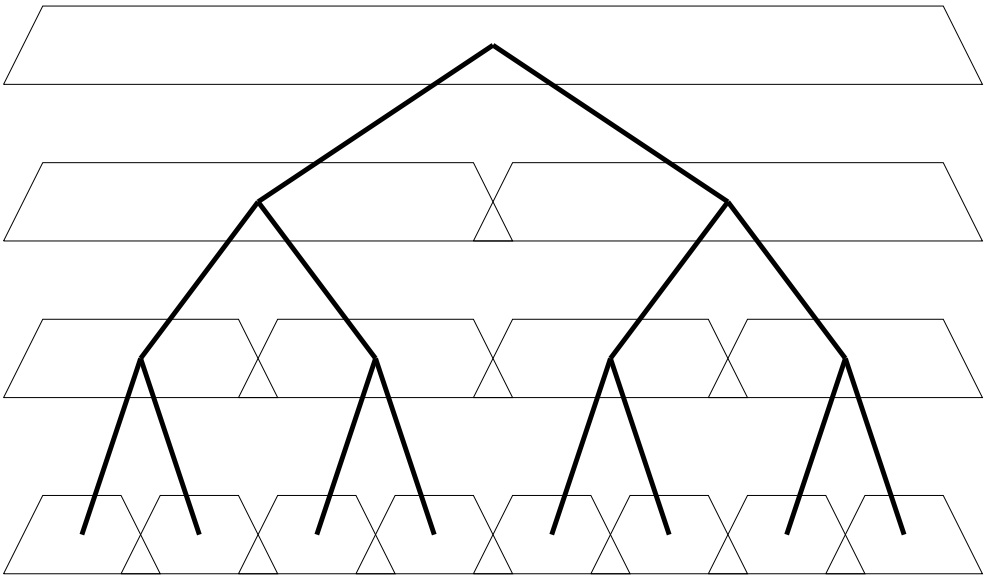

We see that in order to compute the Fourier expansion on the large interval, we can start with adjacent pairs of small intervals, combine coefficients to obtain the expansion on their union, and continue until we reach the largest interval at the top level. Along the way we have obtained all dyadic windowed Fourier transforms as intermediate computations. Clearly every disjoint collection of intervals and their orthogonal bases provides us with an orthogonal basis for the union. A natural question that arises in connection with the windowed Fourier transform is how to place the windows. Comparing Figures 2 and 3 we see the effect of the window selection on the number of large coefficients in the expansion:

Figure 2. Optimal window selection

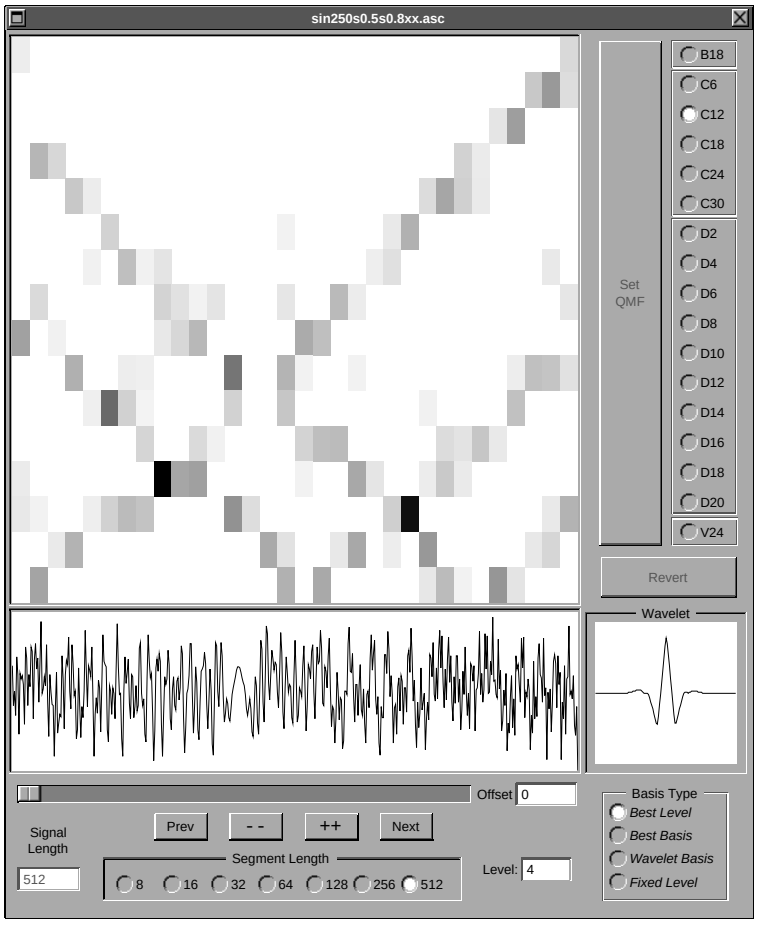

Figure 3. Large window selection

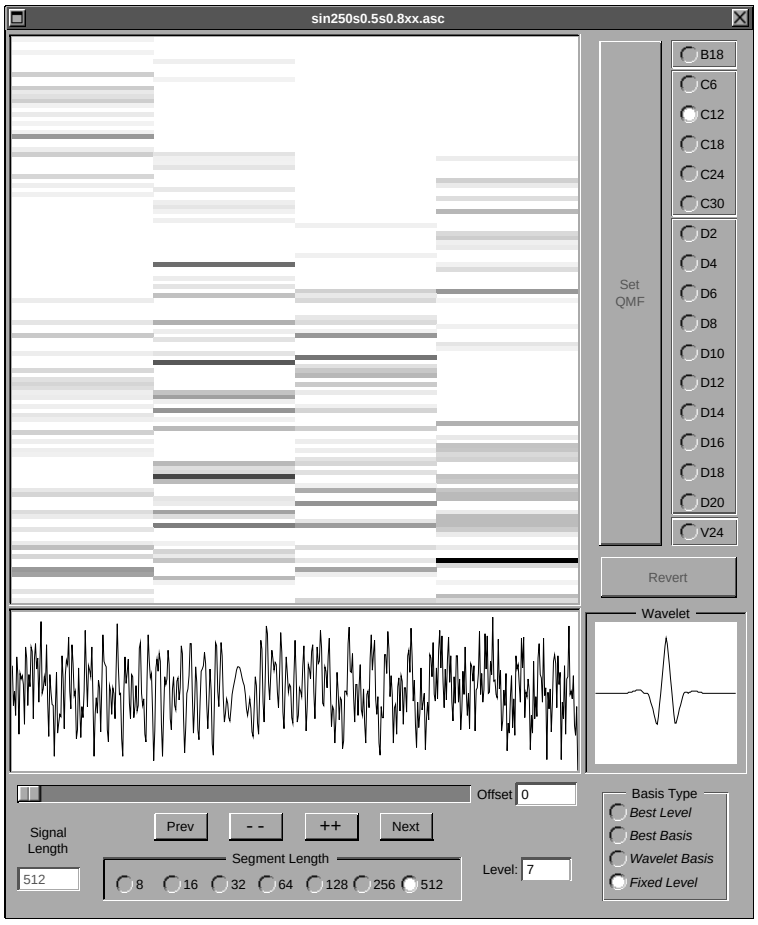

So let us now turn to the question of optimizing the windows to obtain an efficient representation of a function. We can proceed as follows:

We start with the adjacent small intervals and determine the expansion coefficients on each one separately. We then compute the expansion coefficients on the union. Now we can choose that expansion for which the number of coefficients needed to capture 99% of the energy is smallest. Or, we can choose that expansion whose "cost" is smallest: information cost, coding cost, error cost, ...

We compare the cost of the chosen expansions on two adjacent unions of pairs to the expansion on their union and again pick the best.

We continue until we reach an optimal distribution of windows. For example, see Figure

4, where the windows were adapted to digital voice recording.

Figure 4. Adapted window selection for a sound segment

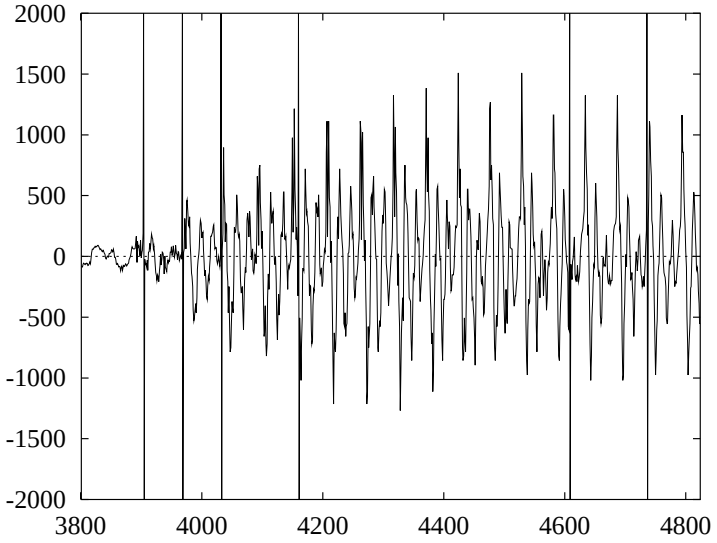

The details of this procedure may be found in [8].

The procedure described above, although natural, is not very useful if we take the windowed Fourier transform with discontinuous windows. The discontinuity introduces "large" expansion coefficients. A cosine basis on each interval is somewhat better. On the other hand, it is well known that we cannot find a smooth window function $\omega(x)$ supported on $(-\frac{1}{2}, \frac{3}{2})$ such that $\omega(x-k)e^{2i\pi nx}$ are orthogonal. (If we could, it would imply that $\int \omega(x)\omega(x-1)e^{-2\pi imx}\,dx = 0$ for all m, and thus $\omega(x)\omega(x-1) \equiv 0$).

Recently Daubechies, Jaffard, Journe [6] and Malvar [7] observed that by taking equal smooth windows and sines or cosines orthogonality can be maintained. Coifman and Meyer [3] observed that the windows can be chosen for different sizes. This enables the adaptive constructions described above and in [2], [8].

Modulated Waveform Libraries. We start by recalling the concept of a "library of orthonormal bases." For the sake of exposition we restrict our attention to two classes

of numerically useful waveforms, introduced recently: *wavelet packets* [2] and *localized trigonometric waveforms* [3].

We start with trigonometric waveform libraries. These are localized sine transforms (LST) associated to covering by intervals of $\mathbf{R}$ or, more generally, of a manifold.

We consider a cover $\mathbf{R} = \bigcup_{-\infty}^{\infty} I_i$, where $I = [\alpha_i \alpha_{i+1})$ and $\alpha_i < \alpha_{i+1}$. Write $\ell_i = \alpha_{i+1} - \alpha_i = |I_i|$ and let $p_i(x)$ be a window function supported in $[\alpha_i - \ell_{i-1}/2, \alpha_{i+1} + \ell_{i+1}/2]$ such that

$$\sum_{-\infty}^{\infty} p_i^2(x) = 1$$

and

$$p_i^2(x) = 1 - p_i^2(2\alpha_{i+1} - x) \quad \text{for} \quad x \quad \text{near} \quad \alpha_{i+1}.$$

Then the functions

$$S_{i,k}(x) = \frac{2}{\sqrt{2\ell i}} p_i(x) \sin[(2k+1)\frac{\pi}{2\ell_i}(x - \alpha_i)]$$

form an orthonormal basis of $L^2(\mathbf{R})$ subordinate to the partition p_i. The collection of such bases forms a library of orthonormal bases [3]. We can likewise form a library of orthonormal local cosine bases:

$$C_{i,k}(x) = \frac{2}{\sqrt{2\ell i}} p_i(x) \cos[(2k+1)\frac{\pi}{2\ell_i}(x - \alpha_i)]$$

Figure 5. Local Cosine Transform (LCT) basis functions

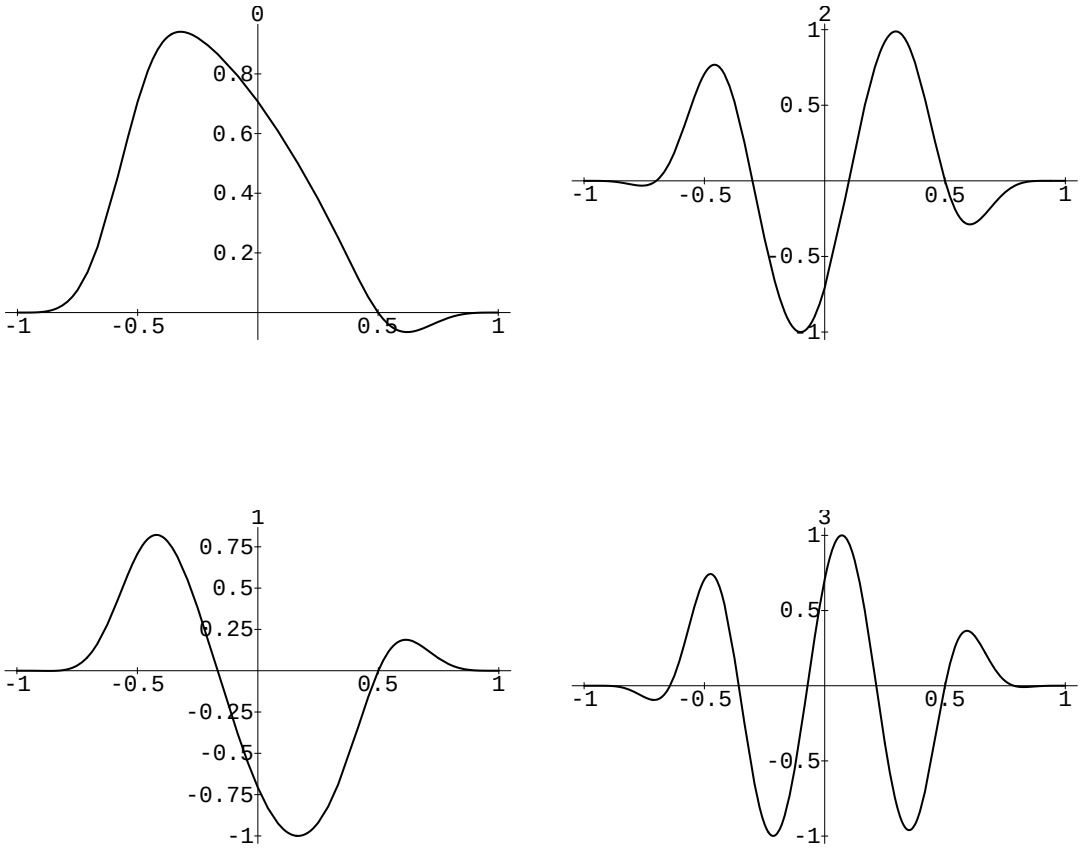

A few of these basis functions are plotted in Figure 5. It is easy to check that if H_i denotes the space of functions spanned by $S_{i,k}$, $k = 0, 1, 2, \ldots$ then $H_i + H_{i+1}$ is spanned by the functions

$$P(x)\,\frac{1}{\sqrt{2(\ell_i + \ell_{i+1})}}\,\sin[(2k+1)\frac{\pi}{2(\ell_i + \ell_{i+1})}(x - \alpha_i)]$$

where

$$P^2 = p_i^2(x) + p_{i+1}^2(x)$$

is a "window" function covering the interval $I_i \cup I_{i+1}$.

Relation to Wavelets and Wavelet Packets. We consider the frequency line $\mathbf{R}$ split as the union of $\mathbf{R}^+ = [0, \infty)$ and $\mathbf{R}^- = (-\infty, 0)$. On $L^2(\mathbf{R}^+)$ we introduce a window

function $p(\xi)$ such that

$$\sum_{k=-\infty}^{\infty} p^2(2^{-k}\xi) = 1 \qquad \text{and} \qquad \operatorname{supp} p(\xi) \subset (\frac{3}{4}, 3).$$

Clearly we can view $p(2^{-k}\xi)$ as window function above the interval $(2^k, 2^{k+1})$ and observe that the functions

$$s_{k,j} = s_{k,j}(\xi) = p(2^{-k}\xi) \sin\left[(j+\frac{1}{2})\pi\left(\frac{\xi - 2^k}{2^k}\right)\right]$$

form an orthonormal basis of $L^2(\mathbf{R}^+)$. Similarly

$$c_{k,j} = c_{k,j}(\xi) = p(2^{-k}\xi) \cos\left[(j+\frac{1}{2})\pi\left(\frac{\xi - 2^k}{2^k}\right)\right]$$

gives another orthonormal basis, but whose elements are not orthogonal to the functions $s_{k,j}$. However, if we define $S_{k,j}$ as the odd extension to $\mathbf{R}$ of $s_{k,j}$ and $C_{k,j}$ as the even extension of $c_{k,j}$, then we find that $S_{k,j} \perp C_{k',j'}$ for all j, k, j', k', permitting us to write $C_{k,j} \pm iS_{k,j} = e^{\pm ij\pi\xi/2^k}\hat{\psi}(\xi/2^k)$ where $\hat{\psi}(\xi) = e^{i\pi/2\xi}p(\xi)$ is the Fourier transform of the Meyer wavelet Ψ defined in [9]. The details of this calculation may be found in [5].

We therefore see that wavelet analysis corresponds to windowing frequency space in "octave" windows $(2^k, 2^{k+1})$.

A natural extension therefore is provided by allowing all dyadic windows in frequency space and adapted window choice. This sort of analysis is equivalent to wavelet packet analysis.

The wavelet packet analysis algorithms permit us to perform an adapted Fourier windowing directly in the time domain by successive filtering of a function into different frequency bands. The dual version of the window selection provides an adapted subband coding algorithm.

The wavelet packet library is constructed by iterating the wavelet algoritm. This library contains the wavelet basis, Walsh functions, and smooth versions of Walsh functions called wavelet packets [2].

Figure 6. Wavelet packets

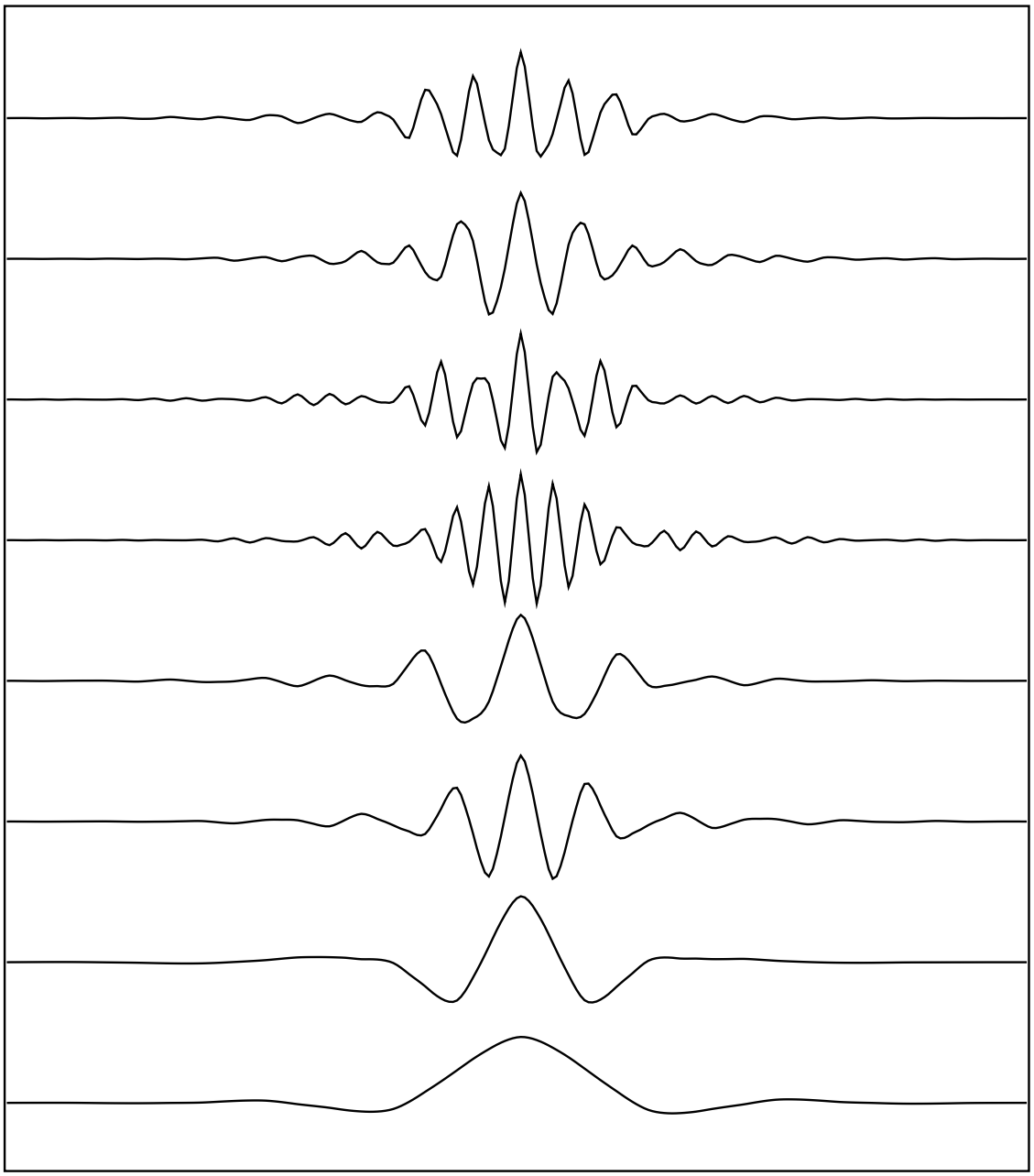

These waveforms are mutually orthogonal; moreover, each of them is orthogonal to all of its integer translates and dyadic rescaled versions. The full collection of these wavelet packets (including translates and rescaled versions) provides us with our library. We may think of these functions as templates or musical notes which we try to match efficiently to

signals for analysis and synthesis [2],[4].

We were led to measure the "distance" between a basis and a function in terms of the Shannon entropy of the expansion. This distance measures the efficiency of a paticular basis for expanding a given function, in rough terms by judging one expansion to be more efficient than another if its coefficients decrease to zero more rapidly.

More generally, let H be a Hilbert space. Let $v \in H,\ \|v\| = 1$ and assume $H = \oplus \sum H_i$ is an orthogonal direct sum. We define

$$\varepsilon^2(v, \{H_i\}) = -\sum \|v_i\|^2 \ell n \|v_i\|^2$$

as a measure of distance between v and the orthogonal decomposition. Then ε^2 is characterized by the Shannon equation which is a version of Pythagoras' theorem.

If we let $H = \oplus(\sum H^i) \oplus (\sum H_j) = H_+ \oplus H_-$, where H^i and H_j give orthogonal decompositions $H_+ = \sum H^i$, $H_- = \sum H_j$, then

$$\varepsilon^2(v; \{H^i, H_j\}) = \varepsilon^2(v, \{H+, H_-\} + \|v_+\|^2 \varepsilon^2 \left(\frac{v_+}{\|v_+\|}, \{H^i\}\right) + \|v_-\|^2 \varepsilon^2 \left(\frac{v_-}{\|v_-\|}, \{H_j\}\right)$$

This is Shannon's equation for entropy, if we interpret as in quantum mechanics $\|P_{H_+} v\|^2$ as the "probability" that v lies in the subspace H_+; this equation enables us to search for a lowest-entropy expansion of a signal, as described in [8].

Wavelet packet expansions correspond algorithmically to subband coding schemes and are numerically as fast as the "fast" Fourier transform (FFT). This is true even if we include the complexity of the search for the lowest entropy wavelet packet basis for a given signal or ensemble of signals.

Time-Frequency Analysis. To each wavelet packet or local trigonometric function we can associate a time t and a frequency f. These will be uncertain by amounts Δt and Δf, respectively, and Heisenberg's uncertainty principle requires that $\Delta t \cdot \Delta f \geq 1$. The result may be interpreted as a rectangular patch of dimensions Δt by Δf, located around (t, f). We shall call the patch a *Heisenberg cell*; it may be shaded in proportion to the amplitude of the corresponding wavelet packet or local cosine component.

Figure 7. Cells in the phase plane

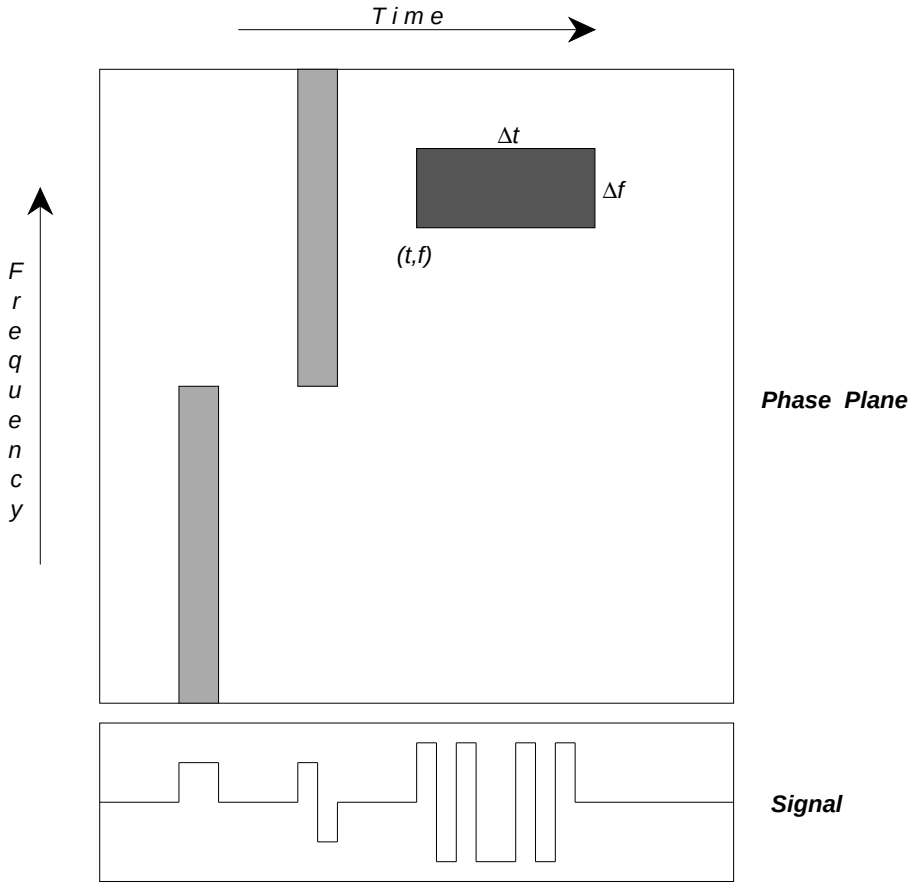

If we choose basis elements which are near-optimally localized in both time and frequency (i.e., for which $\Delta t \cdot \Delta f \approx 1$) then we may depict a basis as a cover of the phase plane by cells of unit area. An orthonormal basis of such *time-frequency atoms* corresponds to a disjoint cover of this idealized phase plane by unit-area cells. Strictly speaking, this corresondence applies to arbitrary disjoint dyadic covers only in the case of the Haar-Walsh or Shannon wavelet packet libraries. The LST and wavelet packet libraries give orthonormal bases only if constrained to certain subsets of the disjoint dyadic covers, since they correspond to a segmentation in space followed by an expansion in frequency, or restriction to a band of frequencies followed by an expansion in space.

Certain bases have characterizations in terms of the shapes of the cells. In Figure 8 we

see that the standard basis (in the finite-dimensional case) has optimal time localization and no frequency localization, corresponding to maximally tall and thin cells arranged in one row, while the (discrete) Fourier basis has optimal frequency localization but no time localization, corresponding to maximally short and wide cells stacked into a single column.

Figure 8. Phase plane decomposition by the standard and Fourier bases

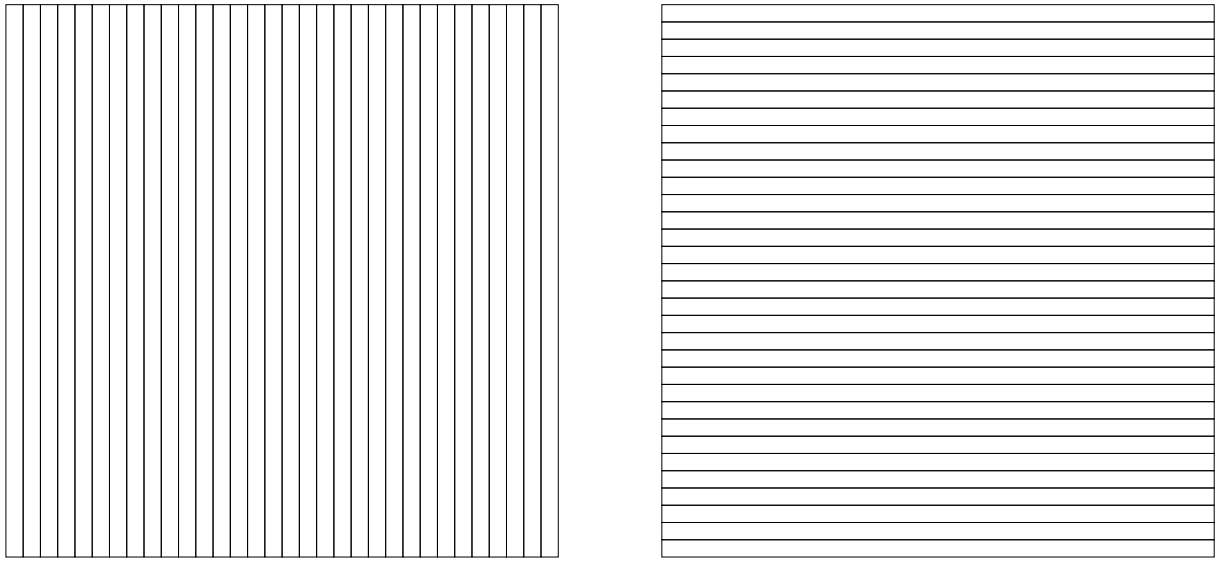

The wavelet basis is an octave-band decomposition of the phase plane, depicted by the cover in Figure 9.

Figure 9. Phase plane decomposition by the wavelet transform

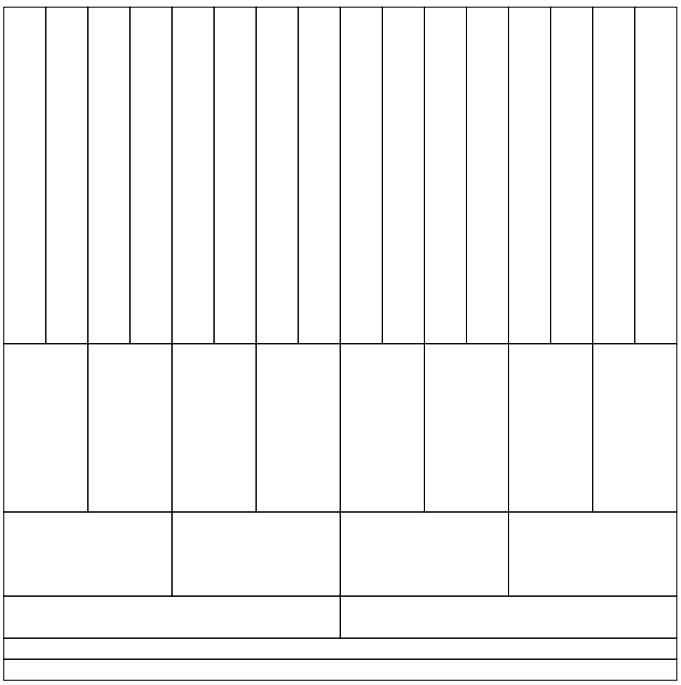

The best-basis of wavelet packets fits a cover to the signal so as to best concentrate the shading into the fewest Heisenberg cells. The compressibility of a sampled signal is easily seen to be the ratio of the total area of the phase plane (N for a signal sampled at N points) divided by the total area of the dark cells (each of area 1). This method allows rectangular Heisenberg cells of all aspect ratios. The best-level or adapted subband basis fits a cover of equal aspect ratio rectangles to the signal, so as to best concentrate the shading. We may automatically analyze signals by expanding them in the best basis, then drawing the corresponding phase plane representation. As is clear, the negligible components will not be drawn, as it is not relevant which particular basis is chosen for a subspace containing negligible energy.

Below are certain canonical signals and their automatic analyses by a computer program

"WPLab" [10]. The user selects a quadrature mirror filter from a list of 17 at the right, and the "mother wavelet" determined by that filter is displayed in the small square window at the lower right. The signal is plotted in the rectangular window at bottom, and the phase plane representation is drawn in the large main square window.

We first analyze a relatively smooth transient, spread over 7 samples in a 512 sample signal:

Figure 10. Representing a fast transient

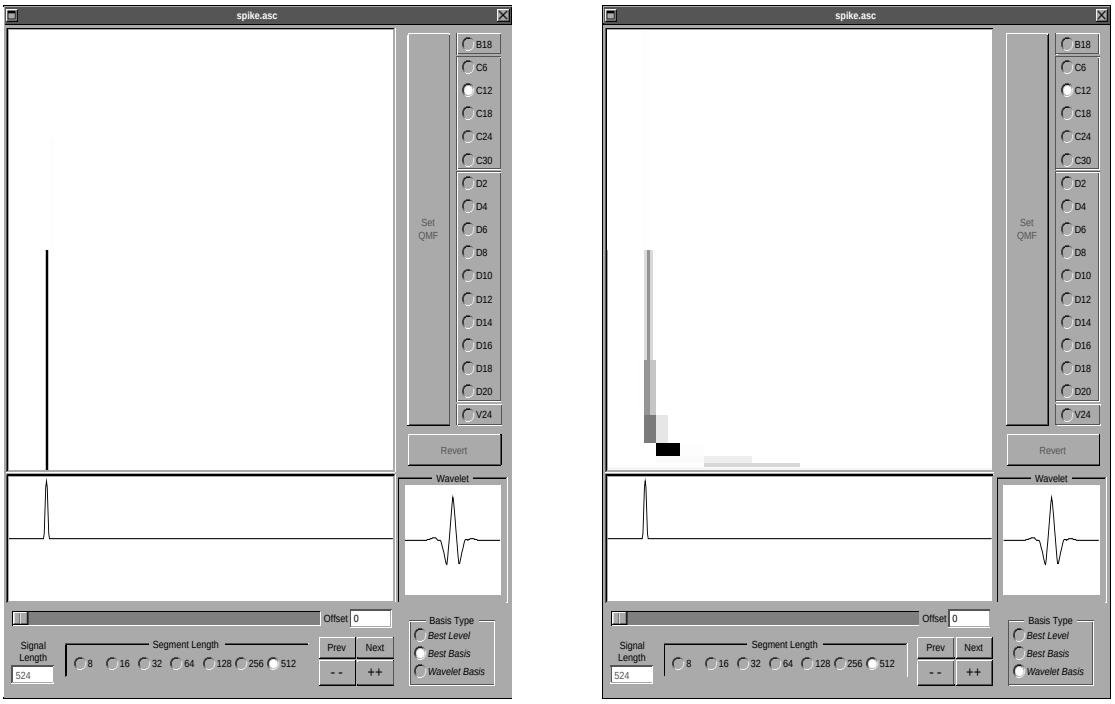

Best basis *Wavelet basis*

Notice that the wavelet analysis at the right correctly localizes the peak in the high-frequency components, but is forced to include poorly localized low-frequency elements as well. The best-basis analysis finds the optimal representation within the library, which in this case is almost a single wavelet packet.

The second signal (in Figure 11) is taken from a recording (at 8012 samples per second)

of a person whistling.

Figure 11. Representing a whistle

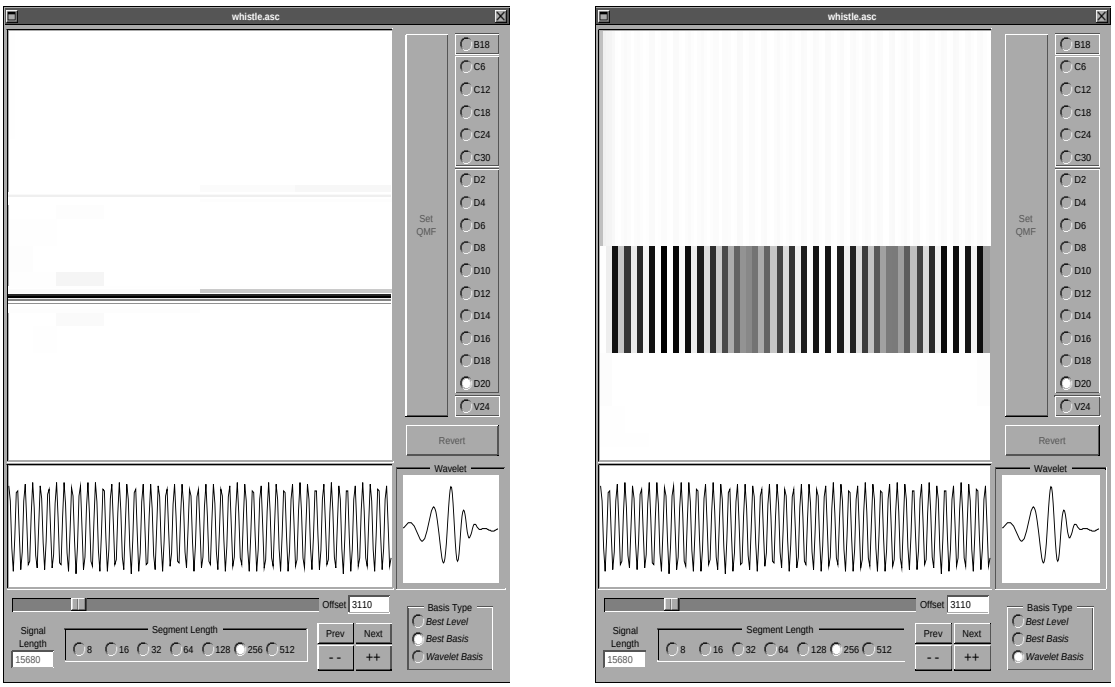

Best basis *Wavelet basis*

Here the wavelet basis is only able to localize the frequency within an octave, even though the best-basis analysis shows that it falls in a much narrower band. The vertical stripes among the wavelet Heisenberg cells may be used to further localize the frequencies, but the best-basis decomposition performs this analysis automatically.

A chirp is an oscillatory signal with increasing modulation. Some examples are the functions $\sin(250\pi t^2)$ and $\sin(190\pi t^3)$, sampled 512 times on the interval $0 < x < 1$ in Figure 12. The modulation increases linearly and quadratically, respectively. The shaded Heisenberg cells in the best bases form a line and a parabolic arc, respectively. In the best-level analyses, all the Heisenberg cells have the same aspect ratio, which is appropriate for a line. In the best-basis analysis, the Heisenberg cells near the zero-slope portion have smaller aspect ratio than those near the large-slope portion.

Figure 12. Linear and quadratic chirps

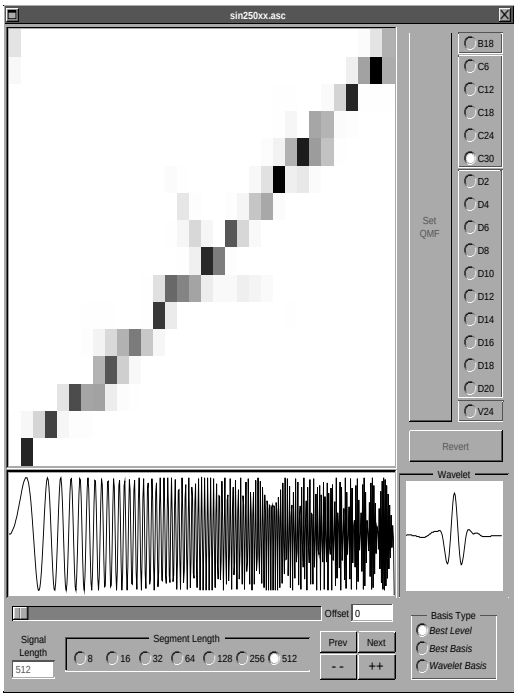

Linear chirp, best level

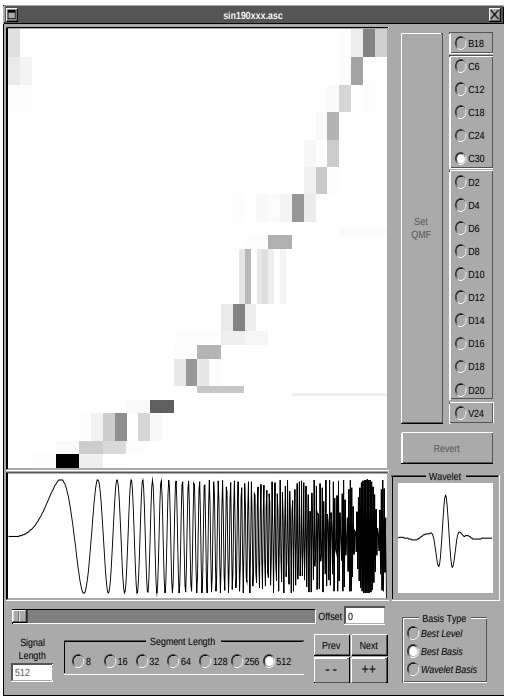

Quadratic chirp, best basis

Such a time-frequency analysis can separate superposed chirps. In Figure 13 we see two pairs of linear chirps, differing either by distinct modulation laws or by a time delay. Both are functions on the interval $0 < t < 1$, sampled 512 times. On the left is the function $\sin(250\pi t^2) + \sin(80\pi t^2)$ analyzed in the best wavelet packet basis. Note that the milder-slope chirp is represented by cells of flatter aspect. On the right is $\sin(250\pi t^2) + \sin(250\pi(t-\frac{1}{2})^2)$, analyzed by best-level wavelet packets. The downward-sloping line comes from the aliasing of neagative frequencies.

Figure 13. Superposed chirps

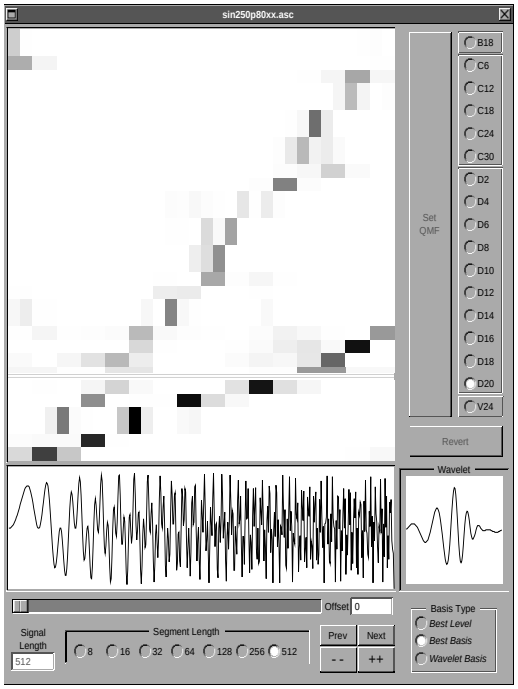

Different slopes, best basis

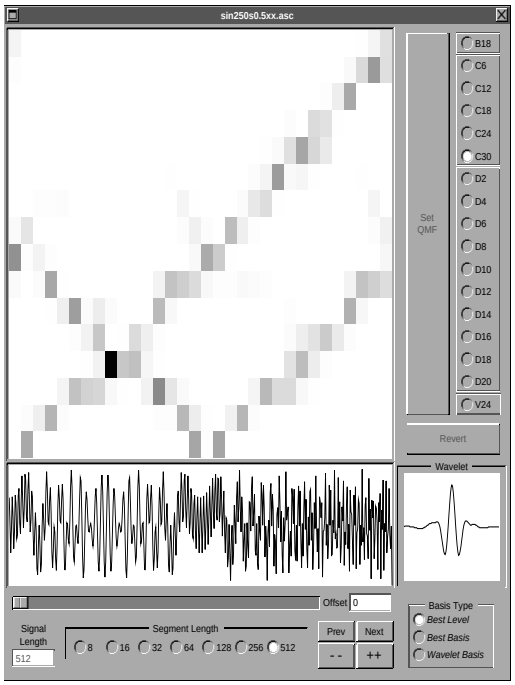

Different phases, best level

Multidimensional Local Trigonometric Transforms. As seen previously, we can partition the time axis into windows with smooth overlap while maintaining orthogonality of smooth localized cosine or sine waveforms.

A similar procedure is possible in higher dimensions either by simply taking tensor products of the bases in each dimension or, more generally, by segmenting the higher-dimensional phase plane into parallelopipeds of prescribed aspect ratios. The only constraint is that we must assure the compatibility of the various window functions.

For definiteness we can start by considering a basis of the form

$$S_{i,k}(x) = \sqrt{2}p(x-i)\sin[(2k+1)\frac{\pi}{2k}(x-i)], \qquad \text{for } i,k \in \mathbf{Z}^+,\ i \geq 0,$$

where $\sum p^2(x-i) = 1$ and p is a bell above $[0,1]$ such that $p^2(x) = 1 - p^2(-x)$ near 0, $1 - p^2(2-x) = p^2(x)$ near 1. Then the bivariate functions $S_{i,k}(x)S_{i',k'}(y)$ form a local trigonometric basis in $\mathbf{R}^2$, based on squares of "size" 1. Assume now that we expand a

function on a square of size 2×2 in terms of this basis based on four subsquares of size 1×1 and compare the "cost" of this expansion to the cost on the parent square, choosing the more efficient expansion. Here the bell function chosen for the square $[0,2] \times [0,2]$ would be $P^{(2)}(x,y) = \sqrt{[p^2(x) + p^2(x-1)][p^2(y) + p^2(y-1)]}$. The choice between parent and children can depend on efficiency in coding, or rate of approximation. Such a procedure can continue for several generations leading to a choice of basis based on squares of different sizes.

We apply this procedure to two bivariate analyses. Figure 14 shows a fingerprint image to be compressed, and Figure 15 shows a matrix to be sparsified. In both of the figures, the selected windows are superposed on the image to indicate how the algorithm chose to segment it.

The adapted box expansion for the matrix in Figure 15, which is derived from an oscillatory-kernel operator useful in the computation of acoustic scattering in two dimensions, provides an efficient way to describe explicitly the interactions between oscillations and geometry. It shows how regions in space need to be coupled to get an efficient description of interactions. The compressed version leads to a straightforward fast numerical algorithm for applying this image viewed as a matrix to a vector [11]. It is the analogue in our new language of the traditional decompositions of operators in terms of both space and frequency localisations, which have a long history in the study of singular integrals and Fourier integral operators.

Figure 14. LCT window selection for a fingerprint compression

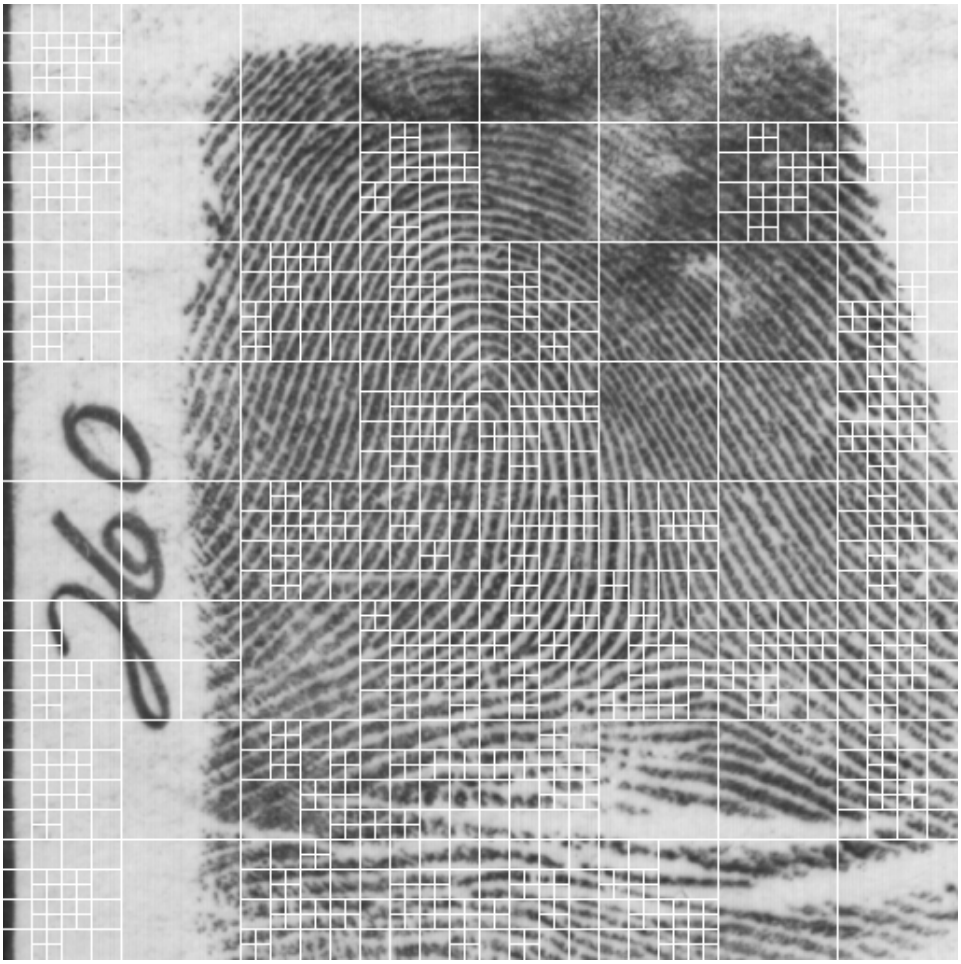

Figure 15. LCT window selection for a matrix compression

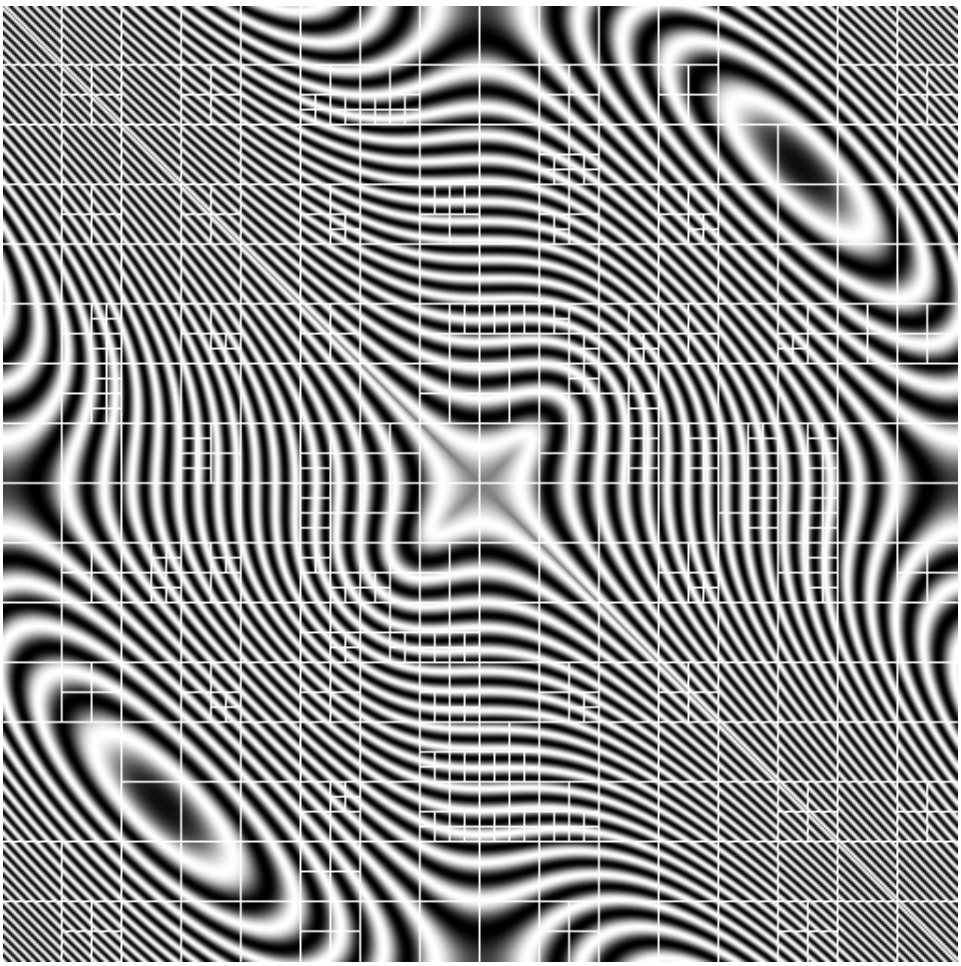

Multidimensional Wavelet Packet Transforms. The quadrature mirror filter algorithm extends to multidimensional signals by separation of variables. The wavelet packets produced by recursive filtering are products of one-dimensional wavelet packets $W_n(x) = \prod_{i=1}^{d} W_{n_i}(x_i)$, together with their isotropic dilations and translations to arbitrary lattice points. Inner products with these multidimensional wavelet packets are computed from averages at the smallest scale, just as in the one-dimensional case. The coefficients may be organized into a stack of d-dimensional intervals, and there is a simple

characterization of orthogonal basis subsets. We can restrict our attention to the case $d = 2$. The diagram in Figure 16 depicts a decomposition of the unit square into a 3-level wavelet packet tree:

Figure 16. 2-dimensional wavelet decomposition to level 3

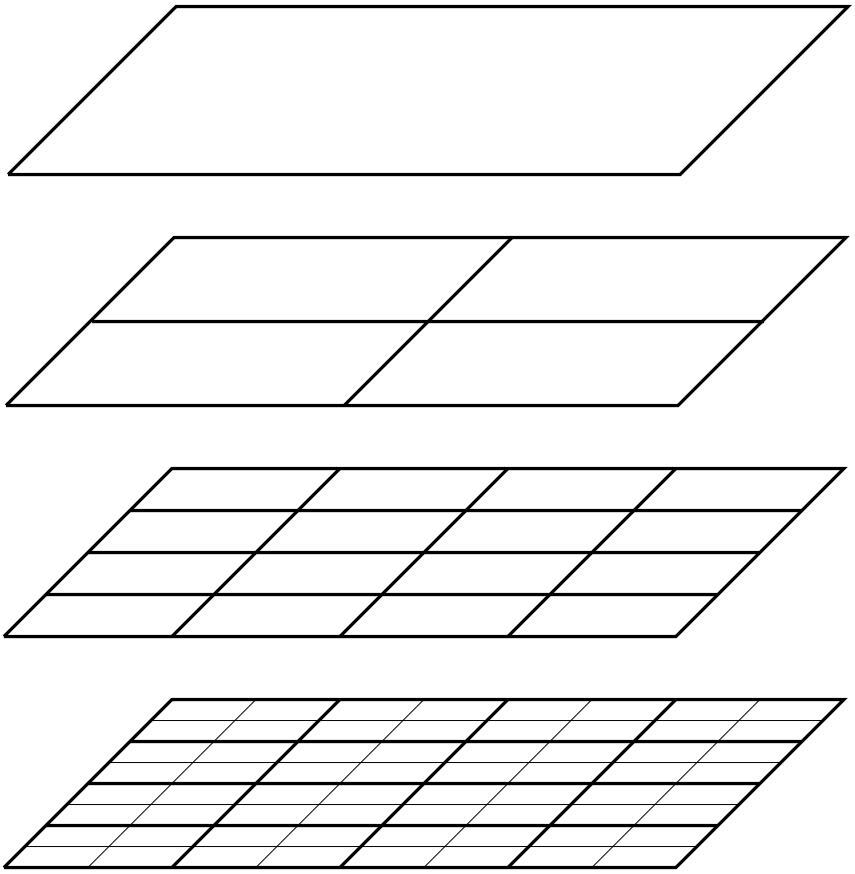

Denoising and Coherent Structure Extraction. As an application combining these ideas we now describe an algorithm for "denoising" or, more precisely, coherent structure extraction. We chose to view a signal f as being noisy or incoherent relative to a basis $\{\omega_i\}$ if it does not correlate well with the waveforms of the basis, i.e., if its entropy is of the same order of magnitude as $\ell g_2 N - \delta$ with small δ, giving a poor compression rate $2^{-\delta}$. From this notion, we are led to the following iterative algorithm based on the several

previously-defined libraries of orthonormal bases.

We start with a signal f of length N, find the best basis in each library and select among them the basis minimizing $\varepsilon(f)$. We reorder the coefficients $\alpha_i = \langle f, \omega_i \rangle$ into decreasing order of absolute value $|\alpha_1| \geq |\alpha_2| \geq \cdots |\alpha_{N_0}|$. We may also assume that each α_i for $i \geq N_0$ is below a precision threshold, for example below 0.1% of the total energy. We then decompose $f = c_M + r_M$, where

$$c_M = \sum_1^M \alpha_i \omega_i, \qquad \text{and} \qquad r_M = \sum_{M+1}^{N_0} \alpha_i \omega_i.$$

We will now say that c_M is coherent and r_M is incoherent if $\varepsilon(r_M) \geq \tau_0$; the threshold τ_0 is chosen to determine if the compression of r_M using $\{\omega_i\}$ is unacceptably bad. We proceed by testing $r_1, r_2, \ldots$ until we reach M for which $\varepsilon(r_M) \geq \tau_0 > 0$, $0 < \tau_0 < 1$, or

$$\sum_{i=M_0+1}^{N_0} \frac{\alpha_i^2}{\|r_M\|^2} \ell g_2 \left(\frac{\|r_M\|^2}{\alpha_i^2} \right) \geq \log_2(N_0 - M_0 + 1) - \log_2 \tau_0.$$

Following the "matching pursuit" procedure described by Mallat, we can now consider r_M as a new signal for which we repeat the decomposition, i.e., we pick a new best basis and decompose $r_M = c'_{M_1} + r'_{M_1}$. We can stop after a fixed number of decompositions, or else we can iterate until no new coherent part is obtained. We then superpose the coherent parts to get the coherent part of the signal. What remains is truly "noise" to us, in the sense that it cannot be well-represented by any sequence of our time-frequency atoms.

The denoising algorithm is depicted in Figures 17–24, which show how a particular signal is peeled into layers as described above. The original signal is a mechanical rumble masked by the noise of aquatic life, recorded through an underwater microphone. The calculations were performed by the program "denoise" [1].

Figure 17. An underwater sound signal

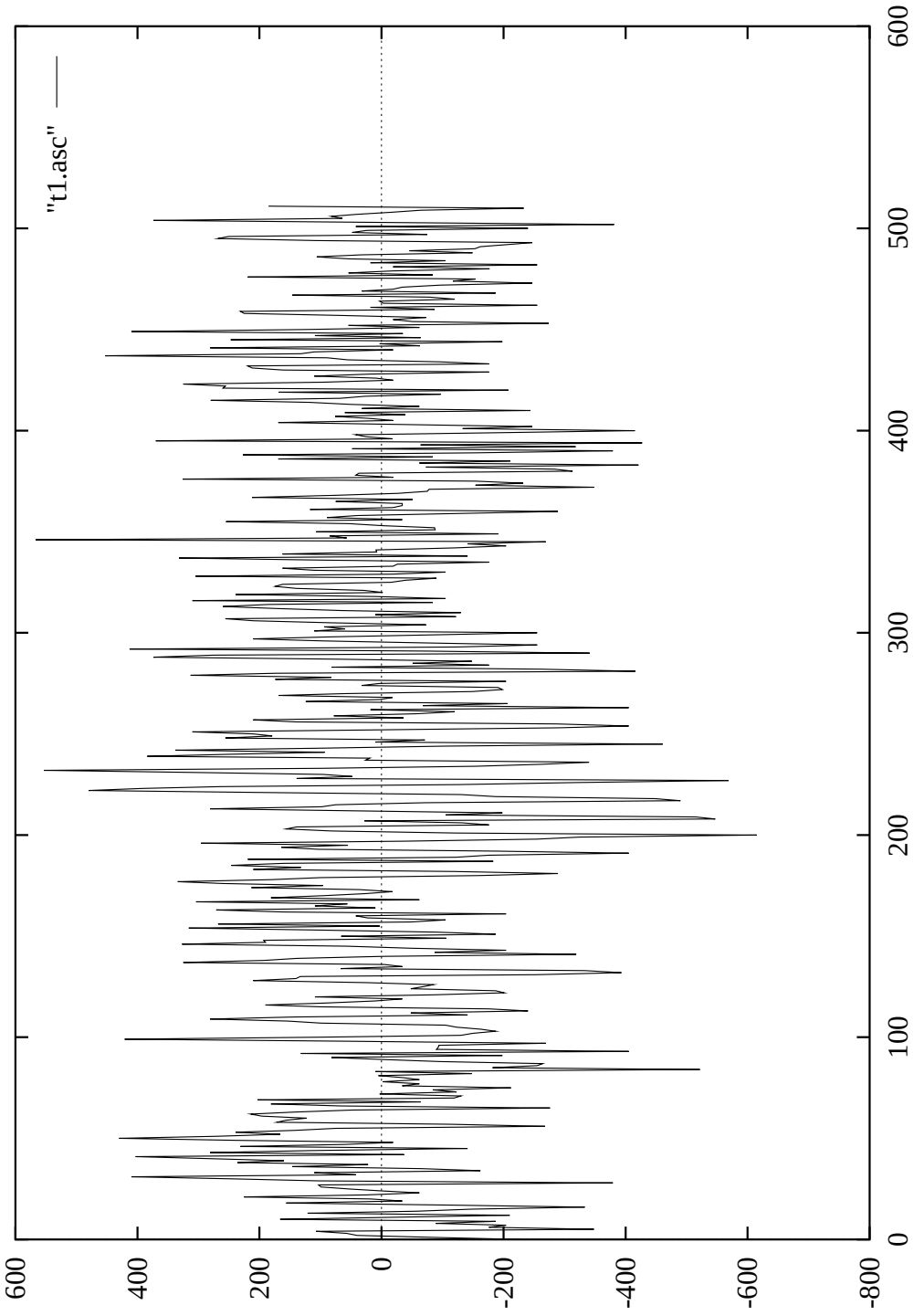

Figure 18. The first coherent component of the underwater sound signal

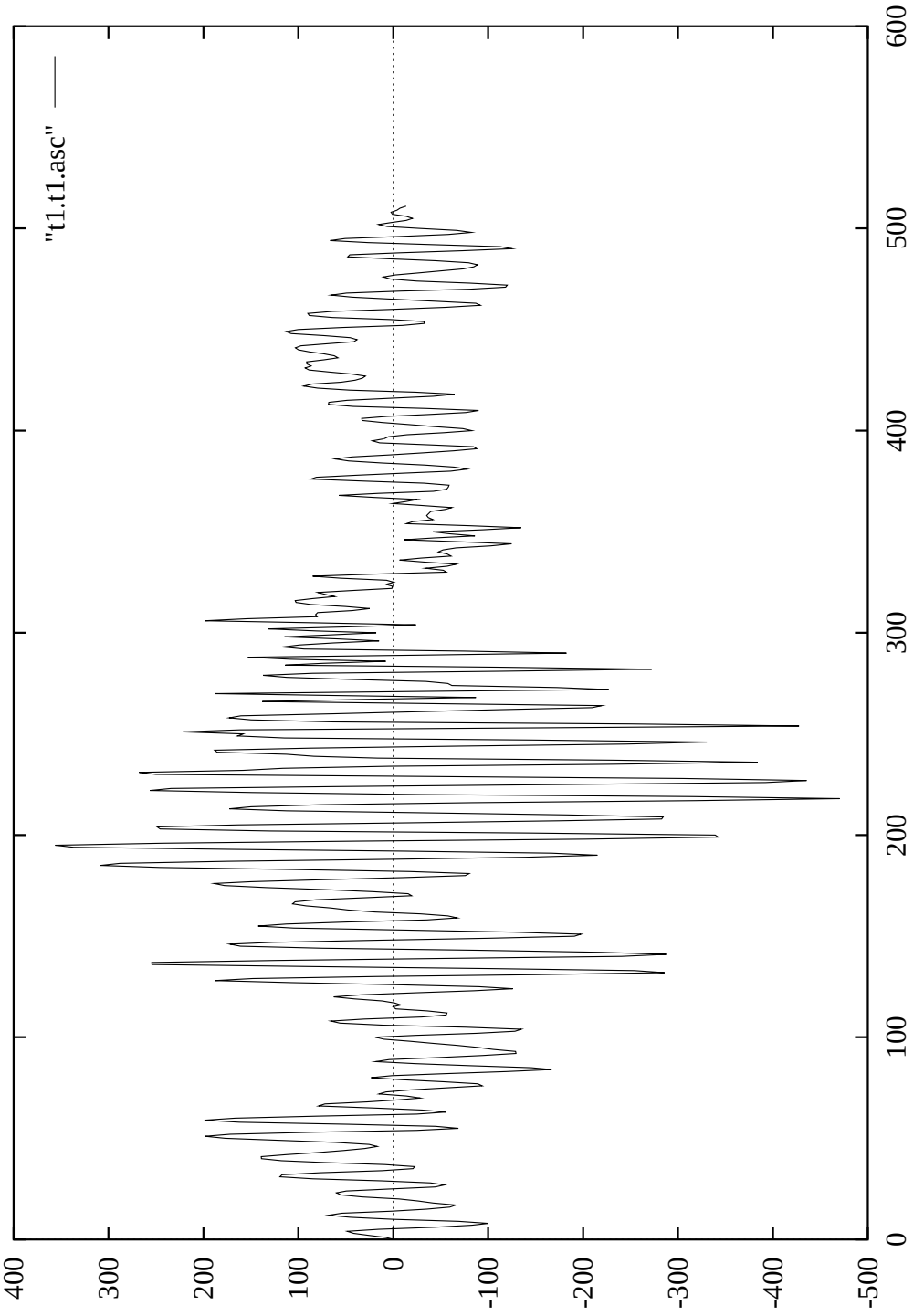

Figure 19. The first noisy residue of the underwater sound signal

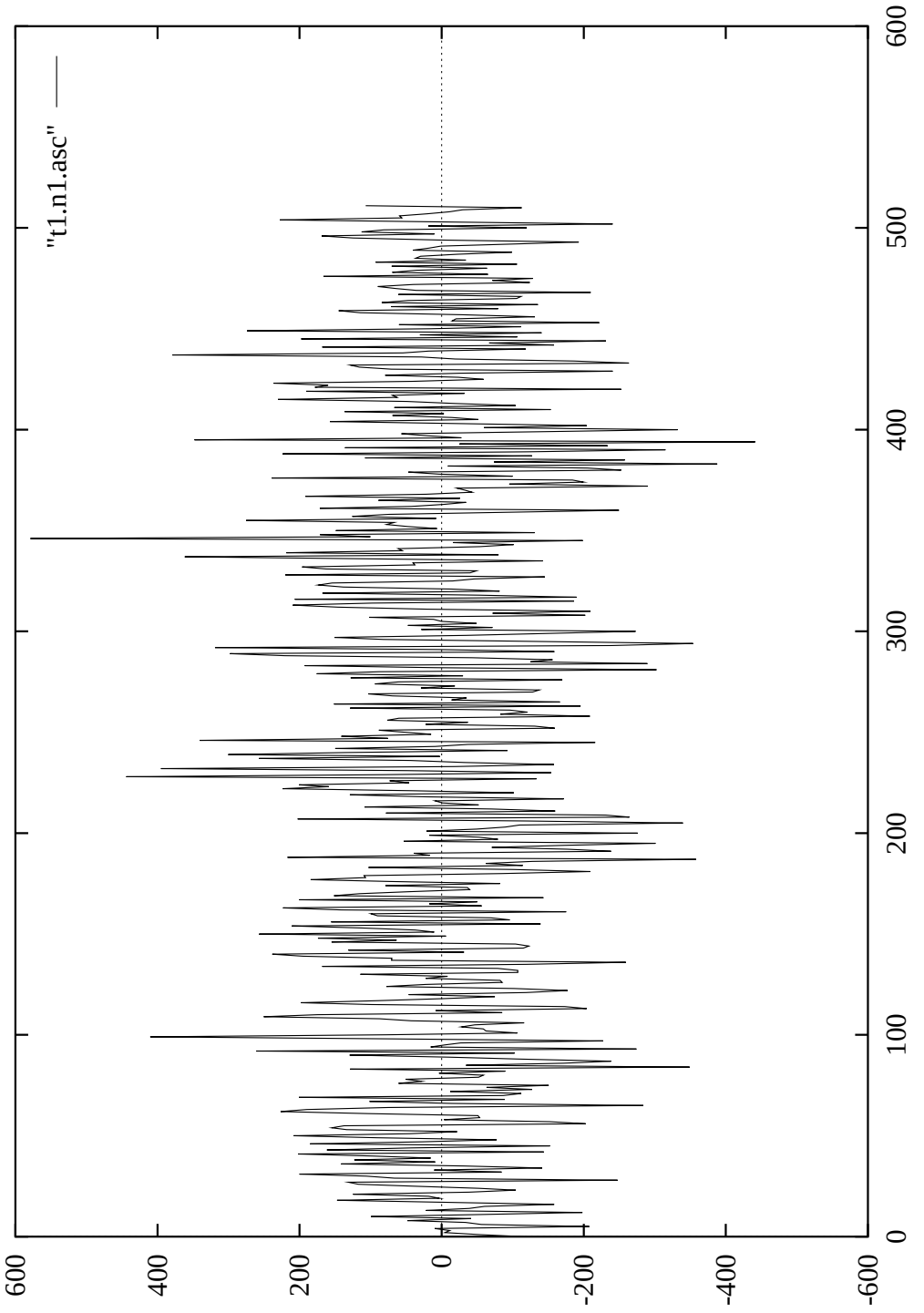

Figure 20. The coherent part of the preceding noisy part

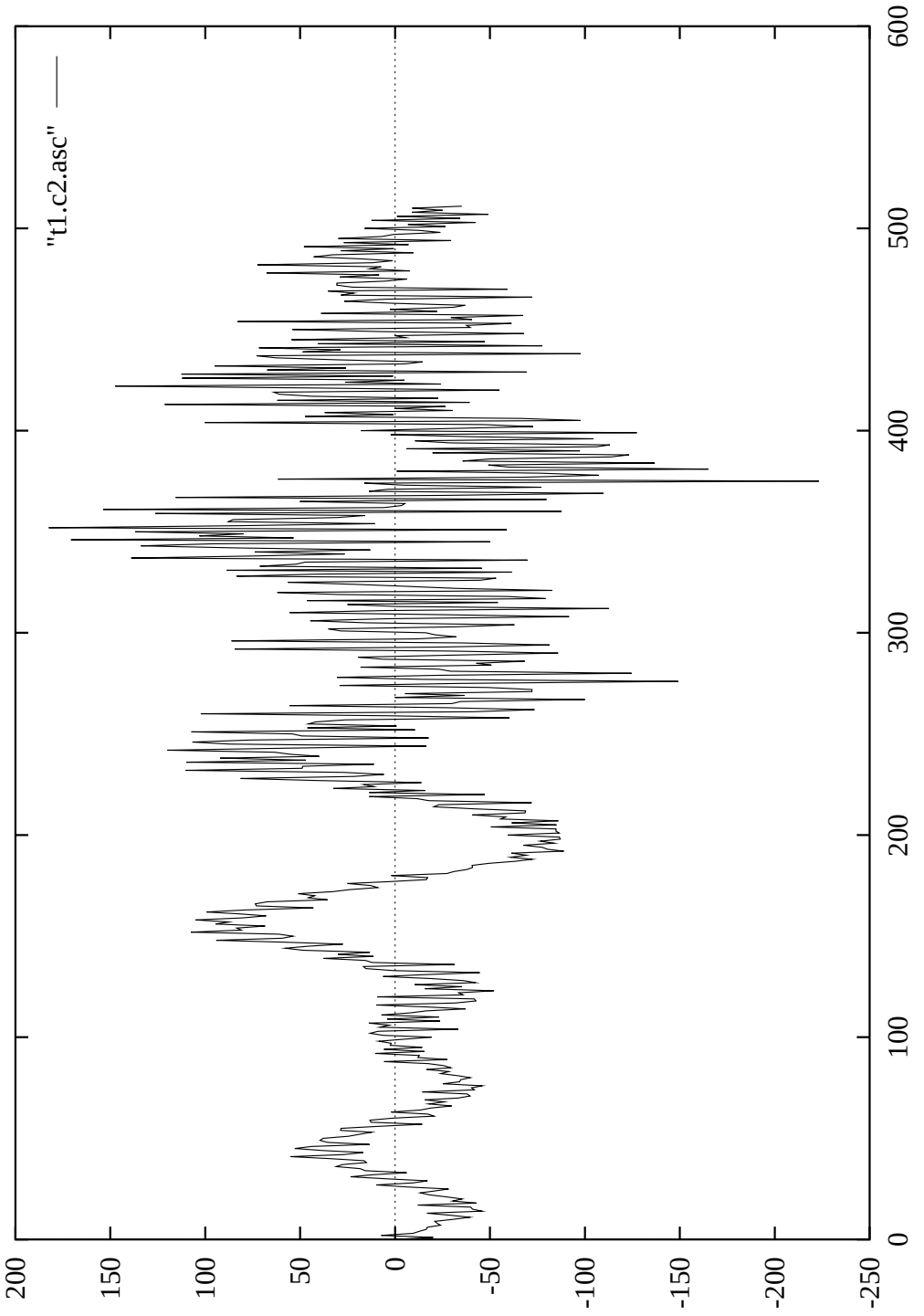

Figure 21. The second noisy component

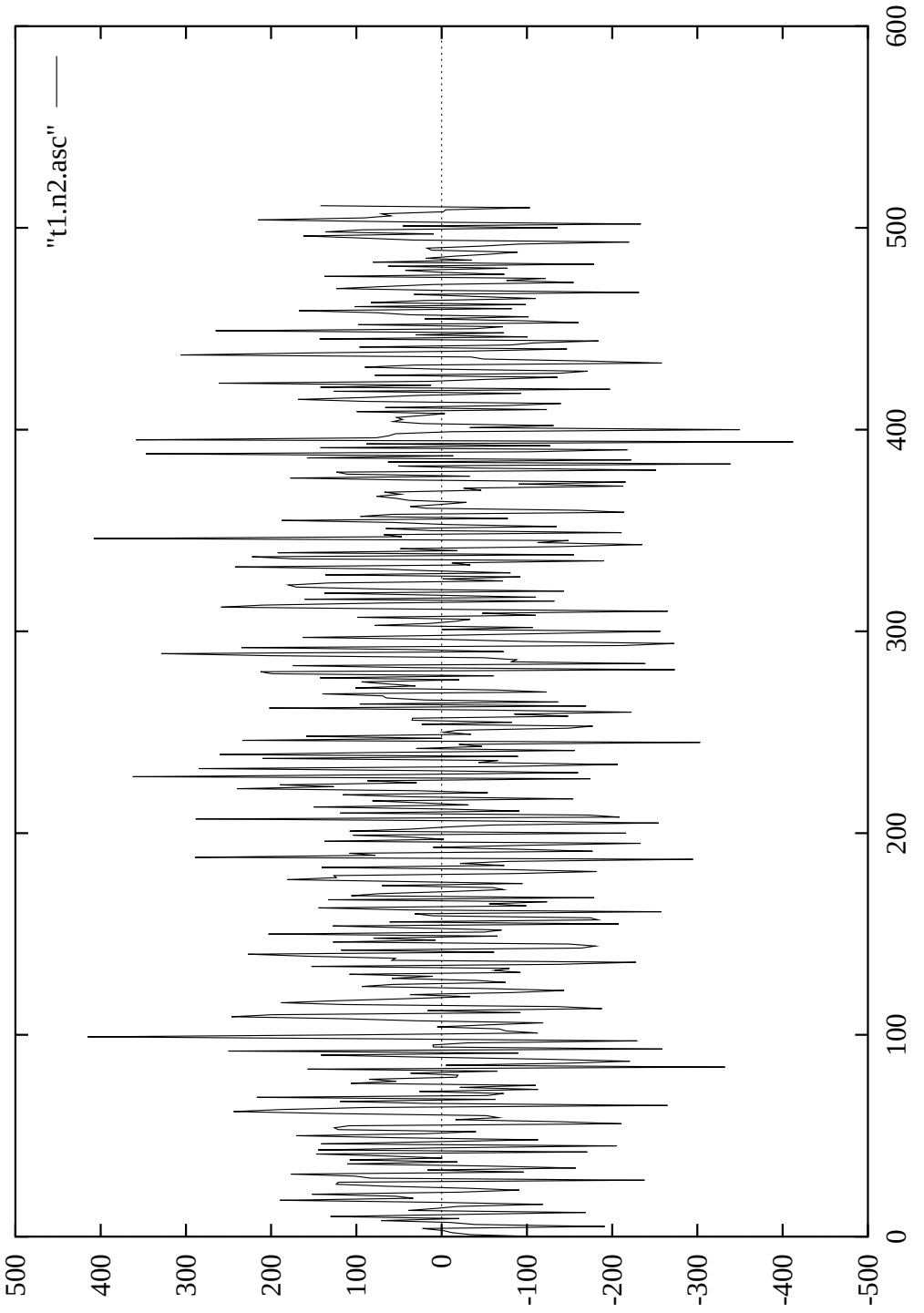

Figure 22. The third coherent component

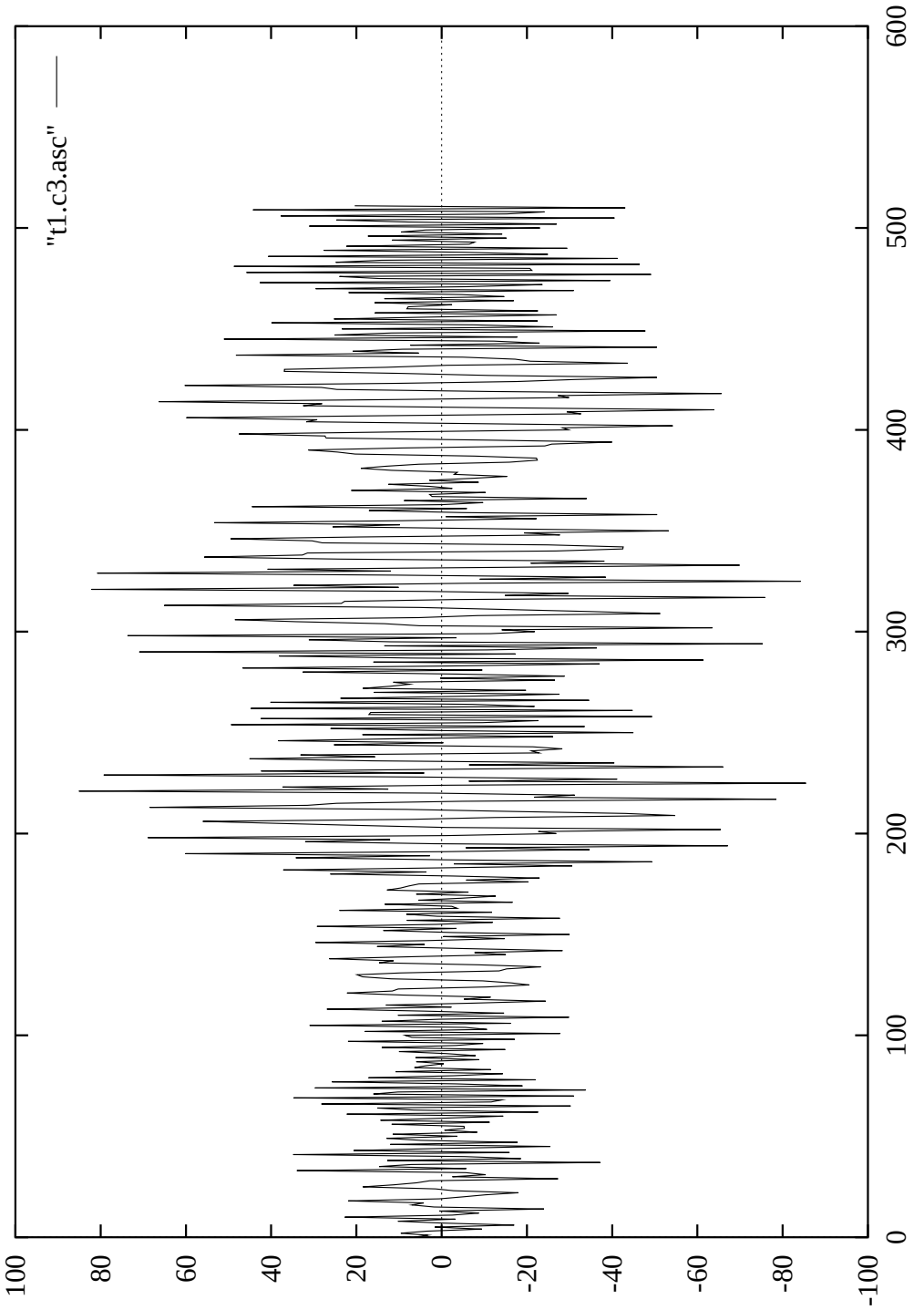

Figure 23. The third noisy component

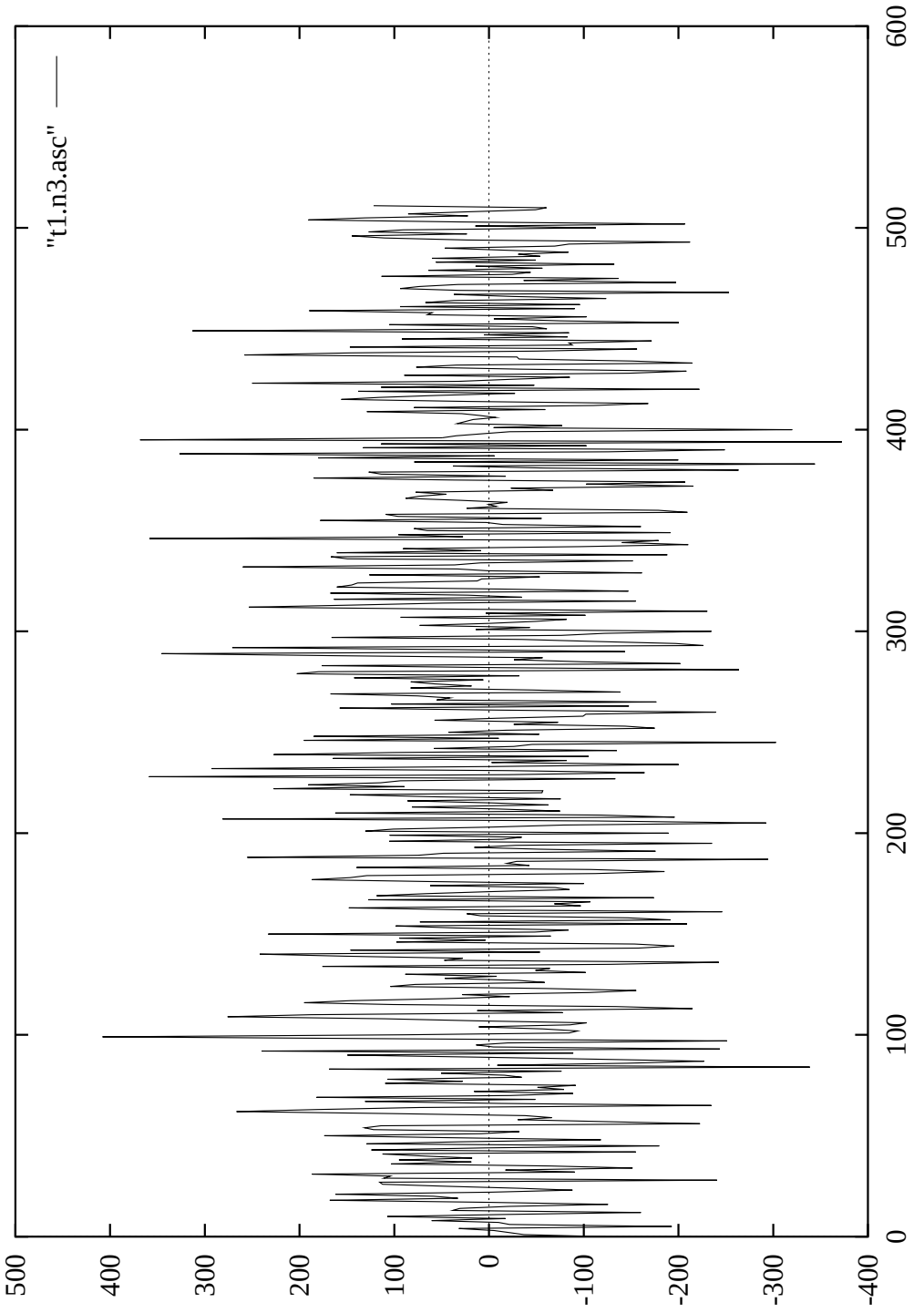

Figure 24. The sum of the coherent parts

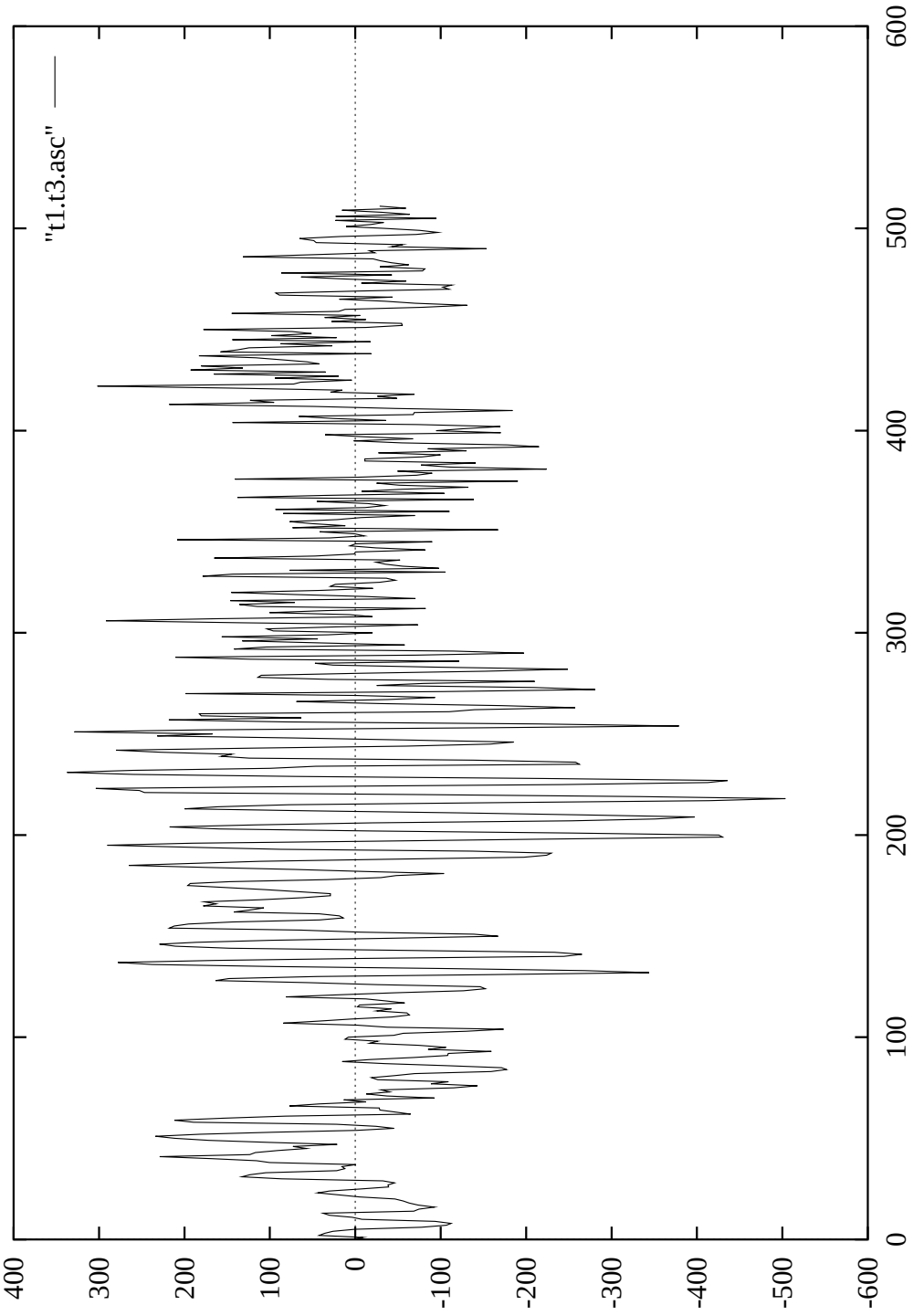

References

1. R. R. Coifman, F. Majid, and M. V. Wickerhauser, *denoise*, Available from FMA&H, 1020 Sherman Ave., Hamden, CT 06514.
2. R. R. Coifman, Y. Meyer, and M. V. Wickerhauser, *Wavelet Analysis and Signal Processing*, Wavelets and Their Applications, Ruskai et al. (ed.); ISBN 0-86720-225-4, Jones and Bartlett, Boston, 1992, pp. 153–178.
3. R. Coifman and Y. Meyer, *Remarques sur l'analyse de Fourier à fenêtre*, série I, C. R. Acad. Sci. Paris **312** (1991), 259–261.
4. I. Daubechies, *Orthonormal bases of compactly supported wavelets*, Communications on Pure and Applied Mathematics **XLI** (1988), 909–996.
5. P. Auscher, G. Weiss, and M. V. Wickerhauser, *Local sine and cosine bases of Coifman and Meyer and the construction of smooth wavelets*, Wavelets–A Tutorial in Theory and Applications, C. K. Chui (ed.) ISBN 0-12-174590-2, Academic Press, Boston, 1992, pp. 237–256.
6. I. Daubechies, S. Jaffard, and J.-L. Journé, *A simple Wilson orthonormal basis with exponential decay*, Also see the "Erratum" on p.878, SIAM J. Mathematical Analysis **22** (1991), 554–573.
7. H. Malvar, *Lapped transforms for efficient transform/subband coding*, IEEE Transactions on Acoustics, Speech, and Signal Processing **38** (1990), 969–978.
8. R. R. Coifman and M. V. Wickerhauser, *Entropy based methods for best basis selection*, IEEE Transactions on Information Theory **32** (March, 1992), 712–718.
9. Y. Meyer, *De la recherche pétrolière à la géometrie des espaces de Banach en passant par les paraproduits*, preprint, École Polytechnique, Palaiseau, Seminaire équations aux dérivées partielles (1985–1986).
10. M. V. Wickerhauser, *WPLab, version 1.5 for NeXT computers*, Available by anonymous ftp in the folder pub/software, pascal.math.yale.edu (1991).
11. M. V. Wickerhauser, *Computation with Adapted Time-Frequency Atoms*, To appear

in *Proceedings of the International Conference: Wavelets and Applications*, Toulouse, 8–13 June 1992.